Cortical feedback depolarization waves: A mechanism of top-down influence on early visual areas

Per E. Roland*†, Akitoshi Hanazawa*, Calle Undeman*, David Eriksson*, Tamas Tompa*, Hiroyuki Nakamura‡, Sonata Valentiniene*, and Bashir Ahmed*

Divisions of *Brain Research and ‡Developmental Anatomy, Department of Neuroscience, Karolinska Institute, S171 77 Solna, Sweden

Communicated by Ranulfo Romo, National Autonomous University of Mexico, Mexico City, Mexico, June 15, 2006 (received for review March 24, 2006)

Despite the lack of direct evidence, it is generally believed that top-down signals are mediated by the abundant feedback connections from higher- to lower-order sensory areas. Here we provide direct evidence for a top-down mechanism. We stained the visual cortex of the ferret with a voltage-sensitive dye and presented a short-duration contrast square. This elicited an initial feedforward and lateral spreading depolarization at the square representation in areas 17 and 18. After a delay, a broad feedback wave (FBW) of neuron peak depolarization traveled from areas 21 and 19 toward areas 18 and 17. In areas 18 and 17, the FBW contributed the peak depolarization of dendrites of the neurons representing the square, after which the neurons decreased their depolarization and firing. Thereafter, the peak depolarization surrounded the figure representation over most of areas 17 and 18 representing the background. Thus, the FBW is an example of a well behaved long-range communication from higher-order visual areas to areas 18 and 17, collectively addressing very large populations of neurons representing the visual scene. Through local interaction with feedforward and lateral spreading depolarization, the FBW differentially activates neurons representing the object and neurons representing the background.

cortical dynamics | neuron communication | object vision | visual cortex | voltage-sensitive dyes

The current view of perception and cognition is that they rely on three main brain mechanisms, each supported by the existence of particular anatomical connections: bottom up, i.e., processing by early sensory areas, which is conveyed to higher-order areas; lateral processing through horizontal connections within an area; and top-down modulatory influences exerted by the rather extensive anatomical connections from higher-order sensory areas to the cortex in early sensory areas. Despite the fact that these top-down connections have been known for >25 years (1), and despite an overwhelming number of reports in which one could interpret the observations as presumed effects of top-down modulations, there is still no direct physiological evidence revealing the mechanism(s) by which higher-order sensory areas alter the computations of neurons in early sensory areas (2). That is, there is no evidence how, when, and where the top-down inputs alter the computation of neurons in early sensory areas. Further, the relative importance and timing of local lateral computations and top-down effects in previous studies of object perception are not obvious (3–5).

Here, we define top-down modulation as a mechanism by which higher-order sensory areas through their connections influence computations of neurons in early sensory areas. These connections typically target neurons in upper (supragranular) layers or in lower (infragranular) layers within these early areas. Theoretically, it has been proposed that lateral interactions and the eventual feedback from higher-order visual areas would be finely timed to engage a large population of supragranular neurons in areas 17 and 18 in a cooperative computation of the visual stimulus and its surroundings (6). Because it is not known how these long-range communications are organized spatially and temporally, we used the voltage-sensitive dye technique (7) to study the depolarization of neurons in the upper layers of cortex. So far, such studies have been restricted to a single sensory or motor area (8–11). There has been no study in which real-time measurement of the depolarization of the dendrites in the upper layers has been studied for communication between areas in the cortex and especially long-range communications, such as feedback from higher-order visual areas.

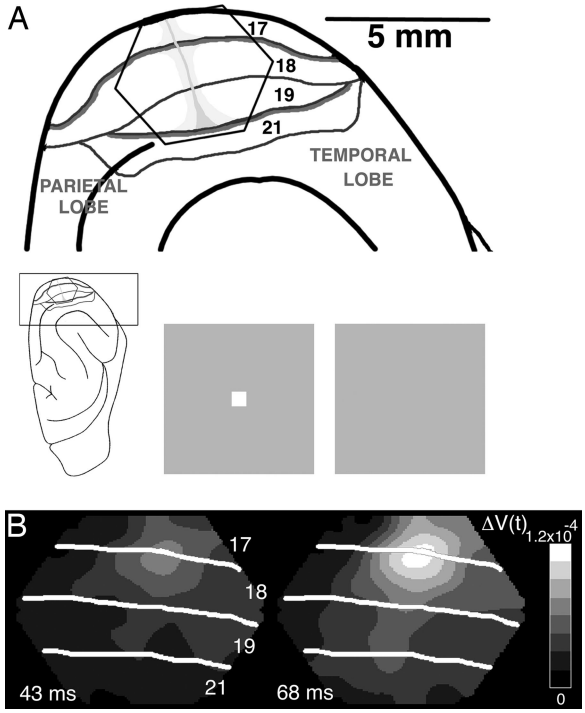

Fig. 1. Experimental setup and visualization of FF and LSD. (*A*) Experimental setup. (*Inset*) The ferret brain with the visual cortex enlarged at the top with the cytoarchitectural areas marked. (*Upper*) The hexagonal photodiode array is shown overlaying visual areas 17, 18, 19, and 21. Each channel of the photodiode array sampled from a cortical area of 150 μm in diameter. The vertical meridians of the field of view are the heavy borders of areas 17/18 and 19/21. The horizontal meridian is light gray and runs orthogonally to the vertical (12). (*Lower*) The stimulus, a 2° × 2° white square or dark gray square (not shown), was presented for 83 ms. The control was a homogenous gray background of the same average luminance. (*B*) FF and LSD. Two frames of the absolute signal $\Delta V(t)$ at the times indicated in milliseconds after the start of the square stimulus. The FF is seen only indirectly in the $\Delta V(t)$, after the depolarizations spread to supragranular layers of cortex.

Conflict of interest statement: No conflicts declared.

Freely available online through the PNAS open access option.

Abbreviations: FBW, feedback wave; FF, feedforward; LSD, lateral spreading depolarization.

†To whom correspondence should be addressed at: Department of Neuroscience, Retzius vag 8, B2:2, Karolinska Institute, S171 77 Solna, Sweden. E-mail: per.roland@neuro.ki.se.

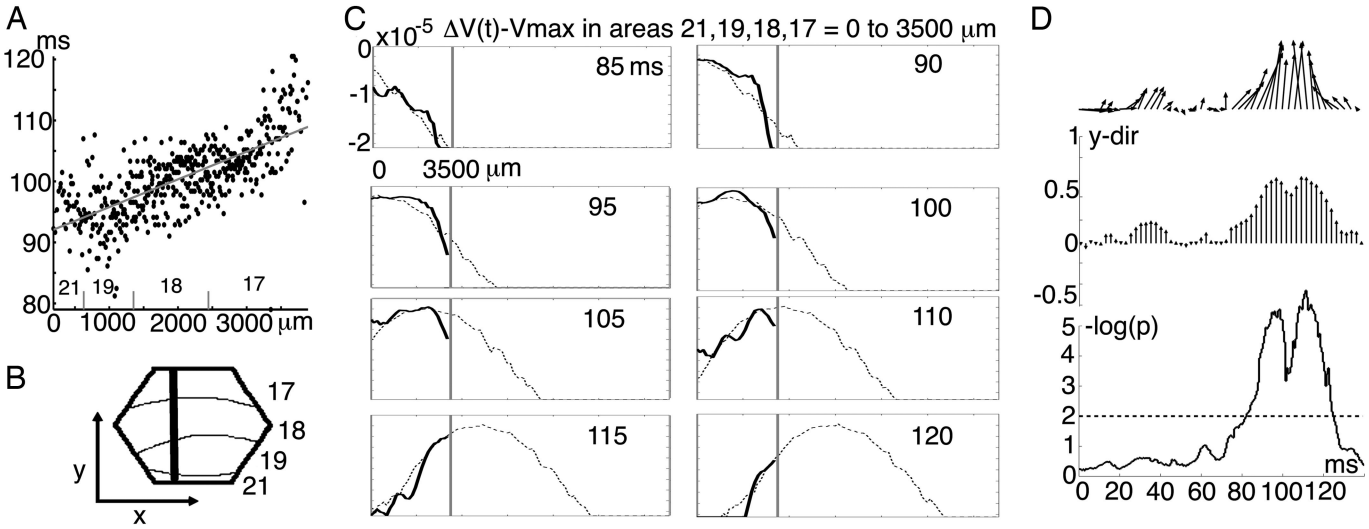

Fig. 2. Wave characteristics of the FBW. (*A*) Testing of significant propagation of the FBW; all channels of the detectors in that animal showing a statistically significant $\Delta V(t)$ were included. Animal 1 is used as an example. The time when the absolute signal of a channel $\Delta V(t)_{xy}$ reaches its maximum is plotted in relation to its position between areas 21 and 17. A linear regression analysis was then performed on each animal, and the estimate of the slope was tested for being significantly >0. The results for all animals are shown in Table 1. (*B*) Mapping of hexagonal array on the cortex of animal 1. The thick line marks the 3,500-μm section from which the data shown in *C* were taken. (*C*) Progression of the FBW along the path shown in *B*. The abscissa from 0 to 3,500 μm corresponds to the path monitored by the detectors. The extra space to the right is virtual, added only to provide the shape of the FBW, because the wavelength is larger than the path. Ordinate: $\Delta V(t) - \Delta V_{max}$, which implies that all values <0. For each time frame of 0.61 ms, the FBW has a profile within the cortex monitored by the detectors. From these profiles in the interval 85–120 ms after the start of stimulus, the mean shape of the FBW was reconstructed and is here shown in gray. The actual profile is shown in black for the time points indicated. Note the steady progression of the FBW (see also Movie 2). (*D*) Direction of the dendritic depolarization across all animals ($n = 11$; see Note 2). (*Top*) The mean direction as a function of time after start of the square stimulus. *B* shows the *x* and *y* directions for the vectors in relation to the cortex. The vector mean was calculated at each time point from the center of the square representation at 17/18 and 60 channels surrounding this center for each animal. The mean of these individual mean vectors was then calculated in a similar way by adding the vectors and dividing by the number of animals. Note the upward direction after 80 ms because of the FBW. (*Middle*) All mean directions projected onto the *y* axis. The ordinate indicates the average length of the *y* vector in proportion to the maximally obtainable *y* vector (i.e., if all animals had a vector pointing directly in the *y* direction, the sum would be = 1). (*Bottom*) −log (*P* values) for consecutive *t* tests along the time axis showing significant feedback depolarization direction only at the time of passage of the FBW (further details in Note 2).

The most remarkable and hitherto unforeseen results were that a short-duration contrast square stimulus (Fig. 1*A*), after a delay, evoked a feedback wave (FBW) of depolarization of the dendrites from higher-order visual areas to lower-order areas 17 and 18. Furthermore, the long-range communication in the form of a FBW is a well behaved broad transient depolarization covering large populations of neurons and carrying an interpretable message to areas 17 and 18. The FBW arrived when the horizontal interactions in the form of a lateral spreading depolarization (LSD) had engaged the whole of areas 17 and 18. The FBW, superimposed on the LSD and the feedforward (FF) input, differentially depolarized the cortical representation of the square and the adjacent cortical representation of the background.

Results

With the presentation of a single contrast square centrally in the visual field close to the crossing of the horizontal and vertical meridians, the absolute voltage-sensitive dye signal, $\Delta V(t)$, mapped the representation of the square at the area 17/18 border in all animals (Fig. 1). $\Delta V(t)$ originates mainly in layers I–III, the supragranular layers of the cortex (10, 13, 14). The increase in magnitude of $\Delta V(t)$, at the representation site at the 17/18 border, is probably due to FF depolarization, i.e., afferent signals from lateral geniculate to supragranular layers via cortical layer IV (15). The extension laterally of this depolarization outside the representational sites, the LSD, has been described (8). At ≈70 ms (70.8 ± 5.6 ms mean ± SD), the LSD depolarized most of exposed areas 17 and 18 (Fig. 1*B*).

Approximately 15 ms later, i.e., 80–90 ms after the start of the stimulus, the peak depolarization appeared, starting at the border between areas 19 and 21. The peak moved fast, with an orientation roughly parallel to the area borders, toward area 17 (Movie 1, which is published as supporting information on the PNAS web site). By following the peak depolarization from each of the cortical points monitored, we could establish the existence of a broad FBW traversing from higher-order visual areas 21 and 19 toward lower-order visual areas 18 and 17 (Fig. 2*A*). For each of the 11 animals, we statistically verified that the maximum amplitude of $\Delta V(t)_{xy}$ passed on from higher-order visual areas toward the square representation at the 17/18 border ($P < 0.0002$; see Fig. 2*A* and Table 1, which is published as supporting information on the PNAS web site). The FBW covered the background representation on its way. Because this $\Delta V(t)$ increase (depolarization) traversed across the supragranular layers from higher-order areas 21 and 19 toward lower-order areas 18 and 17, this was by definition a wave of feedback depolarization to the neurons in areas 18 and 17 (16). Consequently, we have termed this a FBW. In what remains of *Results*, we characterize the FBW and its relation to spike activity.

Visualization and Contributions of the FBW. As seen in Movie 1, before the FBW, the FF and LSD produce a landscape of depolarizations varying over the cortical surface. When the FBW arrives, it becomes superimposed on this landscape. Its shape becomes masked by the landscape, and the FBW is seen only because it moves in one direction, faster than the main changes of the depolarization landscape (Movie 1). To visualize the FBW more clearly, we removed the amplitude differences between the different cortical points by channel-by-channel subtraction of the channel peak value $-\Delta V_{xy,max}$ from the signal, $\Delta V(t)_{xy}$, of that channel: $\Delta V(t)_{xy} - \Delta V_{xy,max}$ (Fig. 5, which is published as

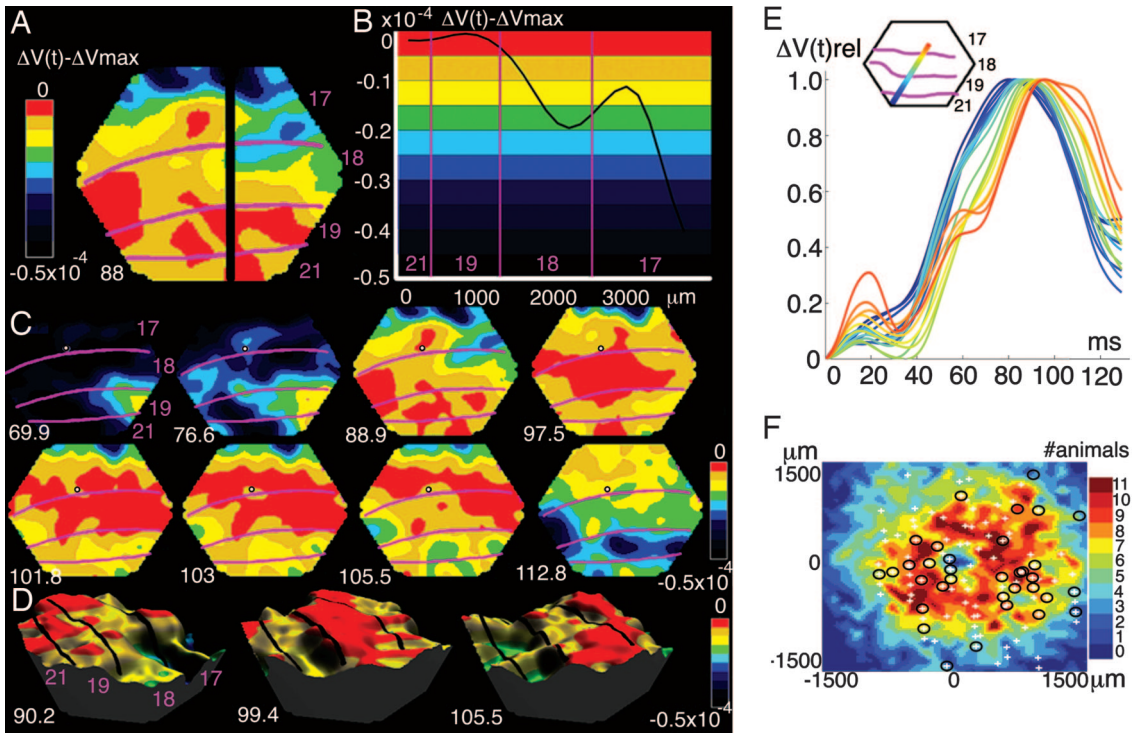

Fig. 3. Spatial characteristics of the FBW. The color coding is identical in *A–D*, as shown by the scales. (*A*) The spatial distribution of the $\Delta V(t)_{xy} - \Delta V_{xy,\max}$ at time 88 ms after the start of the stimulus. Note the FBW reaching first the square representation at the cytoarchitectural border between areas 17 and 18. (*B*) Snapshot of the FBW shape at 88 ms along the black section in *A*. The wavelength is larger than the span of the four visual areas. (*C*) Eight snapshots of the FBW at the poststimulus times indicated in milliseconds. The center of gravity of the square representation is shown with a small circle at the area 17/18 border. The FBW starts at a corner of the temporal lobe (69.9 ms); it runs first to the 19/21 representation and then fast to the 17/18 square representation (76.6 ms), where it maximally depolarizes the square representation (88.9 ms). The $\Delta V(t)_{xy}$ then decreases at square representation (97.5 ms and following frames); later, maximal depolarization of the figure background (101.8–105.5 ms) occurs. FBW maxima surround the 17/18 square representation (103 ms). (*D*) Three snapshots of the FBW passage in 3D for animal 1. (*E*) FBW depicted as a traveling wave propagating in animal 2 along the cortical path (*Inset*). The change in depolarization of each channel is color-coded according to the detector's position in the path (*Inset*). Ordinate: $\Delta V(t)$rel; abscissa, time after start of stimulus. (*F*) The electrode penetration sites in the cortex in relation to the average representation of the square at the area 17/18 border. Axes show the distance from the center of representation. + denotes that no statistically significant spike trains were found; circles denote statistically significant spike trains ($P < 0.001$). Some penetrations had both (circle and +). The square representation was reconstructed from individual animals (for details, see Note 6). Color coding shows the number of animals having the FBW at that cortical point. Shown are 97 penetrations in the cortex representing the background. Of these 97, 30 penetrations show 64 statistically significant multiunits ($P < 0.001$).

supporting information on the PNAS web site). This subtraction sets the maximum values to zero but does not change the temporal dynamics. Now one can see the shape of the wave as it propagates fast from areas 21 to 17 (Figs. 2*C* and 3). The FBW could not be ascribed to the LSD, because this propagates in the opposite direction, from the area 17/18 border toward the area 18/19 border. From the $\Delta V(t)_{xy} - \Delta V_{xy,\max}$ data, we could now estimate the contribution of the FBW to the total signal, because the superimposed FBW showed feedback dynamics, whereas the underlying FF-LSD showed centrifugal dynamics (see Note 1 in *Supporting Text* and Fig. 6, which are published as supporting information on the PNAS web site). Across all animals, the average contribution of the FBW at the square representation site at the 17/18 border was 0.19×10^{-4} or 19.1% ± 6.4% (mean ± SD), and for the background representation along the 17/18 border, it was 0.16×10^{-4} or 27.1% ± 9.8% (the FBW contribution being relatively stronger in the background, $P < 0.02$, $n = 11$; t test, paired two tailed). The FBW has the shape of a wave with a wavelength larger than the distance between areas 21 and 17 (Figs. 2*C* and 3*B*). A FBW with the characteristics depicted in Fig. 3*C* was found in all animals ($n = 11$). These characteristics are seen better in Movie 2, which is published as supporting information on the PNAS web site; the FBW moves within and across the cytoarchitectural borders at constant speed, then first maximally depolarizes the square representation and then the surrounds. The FBW, in interaction with the local FF-LSD, creates a small oblong or rectangular patch or aperture of decreasing $\Delta V(t)$ at the representation of the square. With a delay, a surround of local maximal $\Delta V(t)$ is created in the cortex representing the square background (Fig. 3*C* at 103 ms). The maximum $\Delta V(t)$ at the square representation site in all animals ($n = 11$) always came before the maximal $\Delta V(t)$ of the representation of the background (Fig. 3*F*). On average, the temporal difference measured at peak amplitudes was 8.18 ms (±4.28 ms, SD) at the area 17/18 border ($P < 0.0001$; t test, two tailed; $n = 11$).

Control Measurements and Experiments. Using the vector analysis method on the data (Note 2, and Fig. 7, which is published as supporting information on the PNAS web site.), we detected a significant progress from areas 21 and 19 toward areas 18 and 17 at 80 ms due to the FBW (Fig. 2*D*, Notes 2 and 3, and Fig. 8, which is published as supporting information on the PNAS web site.). The depolarizations caused by the FF and LSD in contrast gave no significant vector direction (Fig. 2*D*). The LSD spread in all directions with an average speed of 0.11 mm · ms^{-1} ± 0.04 mm · ms^{-1} (Note 4, and Fig. 9 and Table 2, which are published as supporting information on the PNAS web site.). The speed of the FBW in contrast was 0.22 ± 0.06 mm · ms^{-1} (mean ± SD; Note 5). The FBW appeared with a latency from 69 to 95 ms ($n =$

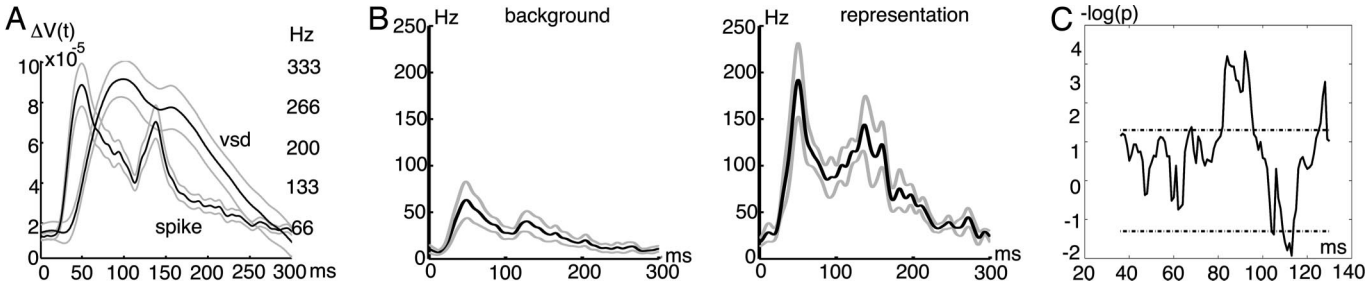

Fig. 4. (*A*) The relation between the $\Delta V(t)$ (vsd) and the spike-firing rate of all multiunits (spike). The $\Delta V(t)$ signals were averaged over all significant channels and subsequently averaged across all animals. The spike-train average was from all significant spike trains. Note the ''on'' response of the multiunits occurs 50 ms in advance of the major increase in $\Delta V(t)$, and that the ''off'' response occurs after the FBW has terminated. Ordinates, $\Delta V(t)$; spike-firing rate in Hz; abscissa time from start of stimulus in milliseconds. The standard errors of the dye signal and the spike trains are shown as gray lines. (*B*) Average spike-firing rate for all background neurons (irrespective of position in cortex) in Hz and average spike-firing rate of all 40 multiunits at the square representation in area 17/18. SEM are shown as gray lines. (*C*) Background neurons firing at the time of passage of the FBW (Note 7). Continuous *t* tests, millisecond per millisecond from 40 to 130 ms after start of square stimulus, if the slope of the regression of peak spike-firing rate against cortical position from areas 19 to 17 is significantly >0. Stippled lines, 0.05 criterion. Note that the slope is significantly >0 only at the time of passage of the FBW, i.e., from 82 to 96 ms. −log (p) gives the negative logarithm of the probability that the regression is different from zero. Note even significant decrease of firing after the time of passage of the FBW.

8). The FBW could be automatically detected with a traveling wave detector (Note 5, and Figs. 10 and 11, which are published as supporting information on the PNAS web site.). In all animals, the FBW was detected as a traveling wave, i.e., having a positive time derivative followed by a wave top and a negative time derivative as it progressed toward area 17 ($n = 11$; $P < 0.0001$; Fig. 3 *D* and *E* and Fig. 12, which is published as supporting information on the PNAS web site; Note 5). It had the same velocity within and across areas with roughly unaltered profile, ruling out depolarization of neurons having different time constants in areas 21, 19, 18, and 1 (Figs. 3*E*, 8, and 11; Note 5; and Movies 2–6, which are published as supporting information on the PNAS web site).

Reversing the contrast of the square to be dark gray compared to the brighter background in four animals resulted in similar FBWs in appearance, course, and speed. Thus the FBW arises no matter whether the luminance of the square was lower or higher than the background (Movie 4). A change in the position of the square along the vertical meridian changed the direction of the FBW ($n = 3$; Movies 5 and 6). If the position of the square was 3.5° below the horizontal meridian, the FBW was directed toward the representation site at the medial part of the 17/18 border (see ref. 12). If the position was 3.5° above the horizontal meridian, the FBW was directed toward the lateral part of the 17/18 border.

The four cardinal characteristics of the FBW are: (*i*) The FBW traverses from higher-order areas depolarizing the neurons over most of the exposed parts of areas 19, 18, and 17, thus covering the representation of the square as well as the background. (*ii*) The FBW contributes the maximal $\Delta V(t)$ increase at the square representation site, and then the $\Delta V(t)$ at this site immediately decreases. This creates a hole or a rectangular aperture matching the square representation, as seen also in the $\Delta V(t)$rel and traveling wave data (Fig. 3 *C*, *D*, and *F*; Figs. 8, 11, and 13; and Movies 2–6). (*iii*) The FBW then, with a delay, contributes to the maximal $\Delta V(t)$ increase of the cortex representing the square background, after which the $\Delta V(t)$ here immediately deceases. (*iv*) The FBW is present in data averaged from stimulus onset.

The existence of the FBW was demonstrated in six different ways: in the absolute signal (Fig. 2, Table 1, and Movie 1), by subtracting $\Delta V_{xy,\max}$ (Figs. 2*C* and 3; Movie 2), by its movement direction (Note 1 and Fig. 6), by the measurement of the direction of the increase in depolarization (Fig. 2*D*), in the $\Delta V(t)$rel (*Methods*, Figs. 3*E* and 4 and Note 3), or by being a traveling wave (traveling wave algorithm, Note 5 and Figs. 10–12). Further, the FBW could be differentiated from the FF-LSD (*i*) by time of onset, (*ii*) by site of origin, (*iii*) by being a traveling wave and not a wavefront or a local increase in $\Delta V(t)$ (Figs. 2, 3, and 11), (*iv*) by direction of propagation (Figs. 2 and 3), (*v*) by spatial course (Figs. 2*C*, 3, 7, and 8 and Movies 1–6), or (*vi*) by its velocity. These properties are incompatible with the FBW being a product of FF depolarization, LSD, or any interactions between LSD and FF.

Relation Between the FBW and the Spiking of Neurons. We electrophysiologically recorded the responses (spikes) from a total population of 104 multiunits, of which 97 were from penetration sites in cytoarchitectural areas 17 and 18. The mean peak-firing rate of these 97 multiunits responding significantly to the square stimulus occurred 50 ms in advance of the peak $\Delta V(t)$ in the supragranular layers (Fig. 4*A*). Furthermore, the mean firing rate from units decreased significantly when the supragranular neurons had their peak $\Delta V(t)$ (Fig. 4*A*). This is compatible with a FF and eventual lateral spread of firing by the neurons in areas 17 and 18 up to 60–70 ms after stimulus onset. This also fits with the appearance of the FBW in the interval 70–110 ms and implies that the spiking activity producing the FBW comes from neurons outside areas 17 and 18. Notably, the earlier decrease of the $\Delta V(t)$ at the square representation cannot be explained by a response to the offset of the square stimulus, because the neurons off response occurs much later (see Fig. 4 *A* and *B*).

The apertures in Fig. 13 (Note 6; see also Fig. 3*F*) were taken as defining the square representation, because they coincided with the representation sites (*Methods*). There were a total of 64 significant spike trains in the cortex representing the background ($P < 0.001$). Raising the criterion to $P < 0.0001$ did not change the number of significant spike trains. The presentation of figure and background together thus increased the firing rate in the background significantly over the rates present when the background alone was presented (Fig. 4*B*). This increased firing rate started during the LSD. A further increase took place at the time of passage of the peak depolarization of the FBW (Fig. 4*C*). After the FBW passage, the firing decreases shortly but significantly (Fig. 4 *B* and *C*).

Discussion

We have demonstrated, in six different ways and with four different statistics, the existence of a top-down feedback traveling increase in $\Delta V(t)$ in the form of a FBW traversing areas 21, 19, 18, and 17 in 11 ferrets. Assuming that the voltage-sensitive dye stained all membranes equally, the $\Delta V(t)$ will be proportional to stained membrane area times the change in membrane

potential (7). A $\Delta V(t)$ increase may therefore reasonably be interpreted as a depolarization of neurons (dendrites and axon terminals; refs. 7 and 11). We have shown that, in response to the presentation of a small square of either higher or lower luminance to the background, most neurons had their peak action potential discharges in advance of the maximal depolarization of the dendrites in layers I–III. This was compatible with the suggestion that these neurons initially conveyed excitation to higher-order visual areas, either outside of the view of the detector array or within this array but mainly to middle and lower cortical layers in areas 18, 19, and 21, the latter termed cortical FF processing. The supragranular cortical dendritic depolarizations first appeared localized to the parts of the visual cortex representing the part of retina stimulated by the square and subsequently spread to the parts representing the background of the square. This was compatible with a thalamocortical FF and subsequent LSD. When the supragranular neurons in areas 17 and 18 were depolarized to 70–80% of their maximal depolarization by the LSD, the FBW arrived, going from higher-order visual areas 21 and 19 toward the area 17/18 border. Thus, being a depolarization traversing across the supragranular layers from areas 21 and 19 over 18 to 17, the FBW is a top-down feedback mechanism well timed to the LSD to bring neurons over their firing threshold. The FBW contributes the maximal depolarization to the representation site of the square and hence the maximal overall depolarization. The membrane potentials then decrease, indicating that the FBW may also cause recruitment of inhibitory neurons.

Characteristics of the FBW as Opposed to Other Depolarizations. In *Results*, we systematically show that the FBW could be separated from the FF and LSD and any interaction between FF-LSD. The FBW could not be due to an off response of the neurons, because it started while the stimulus was still on or before the time that any off signal could have reached the visual cortex (12 ms after stimulus offset in the most-delayed case). Also, we have shown in *Results* that the FBW could not be due to the depolarization of areas 17, 18, 19, and 21 with different time constants. That the FBWs propagate from thalamocortical input, for example, or are related to attention or arousal is incompatible with the cardinal characteristics of the FBW shown by all animals. Specifically, we have shown the FBW within the exposed cortex to be a traveling depolarization wave of high speed, 0.22 mm· ms^{-1}. During its course, it traversed areas having different corticothalamocortical connections, making it unlikely to be of thalamic or corticothalamo-cortical origin (17–19). Its shape (Figs. 2 and 3) and the long delay with which the FBW appears (70–80 ms) corroborated this conclusion. Furthermore, the experimental conditions were against the FBW being due to attention or arousal. Because the animals were anesthetized and the eye muscles paralyzed, the FBW could not arise from attention or eye movements. In addition, the background on the visual stimulator was on between trials, thus eliminating any arousal due to background onsets.

Several authors have described high-amplitude spontaneous depolarizations and cortical waves with velocities >0.1 mm·ms^{-1} in single trial recordings with voltage-sensitive dyes (20–22). Such single-trial spontaneous depolarization waves are not temporally locked to the stimulus. They all have different origins and directions, are slower, and do not show the cardinal characteristics of the FBW (20–22). Consequently, they would be strongly attenuated with the averaging undertaken in our analysis, as will eventual phase shifts of oscillating neurons. Forward-propagating traveling waves of depolarization have been described in the turtle brain as a direct time-locked response to visual input (23, 24). Single top-down feedback traveling waves in the cerebral cortex are difficult to capture electrophysiologically and have not been reported (21).

It might seem surprising that feedback activity is present in the anesthetized state. However, this is not so unexpected, because the anatomical feedback connections are extensive and, when stimulated *in vitro*, give rise to strong and long-lasting depolarizations (25). Also, there is evidence that visual information even in the anesthetized state can reach higher-order visual areas (5). Moreover, our findings are in harmony with the observation in awake animals that local field potentials in upper layers I, II, and III of early visual areas are delayed compared to field potentials in layer IV, the input layer (26).

FBW, One Mechanism of Top-Down Influence on Early Sensory Areas. The FBW is an example of a mechanism of top-down influence on supragranular layers of early sensory areas. Nothing in the recordings from the neurons in areas 17 and 18 indicates they participate in the production of the FBW (Fig. 4). This is in accordance with the FBW being produced by spiking activity outside these areas by means of feedback axons traversing areas 18 and 17 and conveying their synaptic inputs to the dendrites, which then become maximally depolarized. Further observations against an interpretation of the FBW as a polysynaptic feedback, area by area, are that the FBW is a traveling wave with a roughly unaltered profile propagating with high constant velocity within and across area borders. Moreover, the data provided no support for the depolarization of areas 21, 19, 18, and 17 with different time constants in the time interval of the FBW communication. One possibility is that the FBW may be produced by synaptic input to the dendrites in areas 21, 19, 18, and 17 from long-range feedback axons connecting area 21 with area 17 (27). Alternatively, spiking neurons in temporal and parietal lobe visual areas, by their long-range feedback axons, make multiple excitatory synapses in areas 21, 19, 18, and 17 produce the FBW. It remains to be examined whether the neurons producing the FBW synchronize (28).

When figure and background are presented together, the neurons fire with a slight delay significantly in the background domain in areas 17 and 18, most likely because of the LSD (Fig. 4*B*). Figure plus background gave significantly higher firing rates than background alone for the representation of the square as well as for the representation of the background. This could signal information about the whole visual scene to higher-order areas. When the FBW arrives, it depolarizes the representation of the background and of the square, i.e., the whole visual scene. Temporal cortex neurons alone may not be able to compute the segmentation of figure from ground (29). The finding that the FBW consistently makes a temporary aperture that fits the square representation at the 17/18 border (Fig. 3*F*) adds to the already-existing idea that the essential part of figure ground segmentation takes place in areas 17/18 as a consequence of top-down feedback (30). The FBW contributes the maximal depolarization of the neurons at the square representation site on average 8.2 ms before the maximal depolarization of the neurons representing the background. Interestingly, humans can actually segment figure from ground purely by temporal delays between figure and ground down to 10 ms (31). The task of representing both figure and background engages very large populations of neurons in visual areas 17, 18, 19, and 21. The interaction of the FBW with the FF and LSD at and immediately around the square representation in areas 17 and 18 hypothetically could aid the segmentation of figure from ground. Perhaps more important is the result that the long-range communication in the form of the FBW shows well behaved spatiotemporal dynamics that collectively may bind large populations of neurons signaling the visual scene.

Materials and Methods

All experimental procedures were approved by the Stockholm Regional Ethics Committee and were performed according to

European Community guidelines for the care and use of animals in scientific experiments.

Material. Eleven fully anesthetized adult female ferrets (1% isoflurane/50:50 N_2O:O_2) were paralyzed (pancuronium bromide 0.6 mg·kg^{-1}·h^{-1}, i.v.) and artificially ventilated; expiratory CO_2 was measured and kept between 3.3% and 4%. Body temperatures were maintained at 37°C. The exposed visual cortex was stained for 2 h with the voltage-sensitive dye RH795 (Molecular Probes, Leiden, The Netherlands) ($n = 6$) or RH1691 (Optical Imaging, Rehovot, Israel) ($n = 5$). The pupil was dilated (1% atropine sulfate eye drops), and a contact lens was placed over one eye; the other eye was occluded.

The visual stimulus was presented on a computer display and refreshed at 120 Hz, placed at a distance of 57 cm from the animal. The stimulus was a white square (2° × 2°, duration 83 ms, 120 cd·m^{-2}) presented on a uniform gray background (30 cd·m^{-2}; Fig. 1). The square was presented at the center of field of view in all 11 animals, and in three of these animals, in one of three different visual field positions 3.5° apart along the vertical meridian (checked by electrophysiology). The background remained between trials. Four of the five animals stained with RH1691 were in addition stimulated with a dark gray square (10 cd·m^{-2}) against a gray background (60 cd·m^{-2}). Each stimulus was presented five times per session (8–10 sessions per animal).

Voltage-Sensitive Dye Measurements. A WuTech Instruments (Gaithersburg, MD) H469-IV camera with an array of hexagonally arranged 464 photodiode detectors and a Red Shirt Imaging (New Haven, CT) macroscope with ×2 objective were used for optical imaging with a frame every 0.61 ms of the depolarizations from a hexagonal cortical area of diagonal length 4.2 mm (Figs. 1 and 3). The stimulus presentation was synchronized with the ECG signal, and respiration was stopped during stimulus presentation.

Electrophysiology and Anatomy. The action potentials of single/multiple neurons were recorded with thin tungsten electrodes (impedance range, 0.8–1.1 MΩ) in a total of 104 multiunits. Electrode positions were marked, and occasional coagulation marks were left to calibrate the depth measurements from the microdrive. A Poisson distribution was fitted to the spike trains in the prestimulus period and spikes from the background trial. Spike trains passing both the criterion of having significantly increased discharge rate compared to the prestimulus period of $P < 0.01$ and increased rate compared to the background condition of $P < 0.01$ were considered statistically significant periods of firing. After recordings, the brain was sectioned and stained, cytoarchitectonic areal borders were marked, and electrode marks were identified (32). The sections were reconstructed and fitted to the pictures of the operative field and voltage-sensitive dye recording sites to match the electrode penetrations. Note 7 describes the analysis of firing-rate gradients.

Data Treatment of the Voltage-Sensitive Dye Signal. The voltage-sensitive dye signal from the background condition was subtracted from that of the stimulus condition to give for each channel CH: $V(t)_{\mathrm{CH,stim}} - V(t)_{\mathrm{CH,ctl}}$. Reponses from 10–16 subtractions were averaged. From this averaged signal, $\Delta V(t)_{\mathrm{CH}}$ was calculated as the difference in averaged fluorescence to the stimulus minus the fluorescence to the gray screen of same average luminance, divided by the fluorescence obtained in darkness $F0_{\mathrm{CH}}$ for one channel CH: $\Delta V(t)_{\mathrm{CH}} = (V(t)_{\mathrm{CH,stim}} - V(t)_{\mathrm{CH,ctl}}/F0_{\mathrm{CH}}$. For each channel, the average amplitude, C, of $\Delta V(t)_{\mathrm{CH}}$ in the 200-ms prestimulus period was subtracted from the $\Delta V(t)_{\mathrm{CH}}$, i.e., $\Delta V(t)_{\mathrm{CH}} - \mathrm{C} = \Delta V(t)_{xy}$. $\Delta V(t)_{xy}$ is called the absolute signal, and only $\Delta V(t)$ is used unless a particular operation specifically engaging single channels one by one is referred to. Using the amplitude fluctuations in the prestimulus interval to define the noise level, the depolarization signal, $\Delta V(t)$, was thresholded at $P < 0.002$ or less of being noise (uncorrected for multiple tests). The prerequisite for entering the study was that the recording should have a statistically significant $\Delta V(t)$ in response to the square stimulus. Peak latencies were measured on time derivatives of the $\Delta V(t)$, i.e., the time point when the $dt\Delta V(t)$ crosses zero after having been positive. To study phase relations, we calculated the relative amplitude for the poststimulus interval, i.e., from 0 to 200 ms after the start of the stimulus for each statistically significant channel $\Delta V(t)_{xy,\mathrm{relative}} = (\Delta V(t)_{xy} - \Delta V(t)_{\mathrm{min}})/(\Delta V(t)_{xy,\mathrm{max}} - \Delta V(t)_{xy,\mathrm{min}})$. In the text index, *xy* is suppressed and given as $\Delta V(t)$rel.

Representational Sites. The estimated space occupied by the square representation at the area 17/18 border was a rectangle of 4 × 1.5 channels (from ref. 12). Therefore, the square representation site was defined as the four to six maximally depolarized channels here. The apertures in Note 8 coincided with the square representation. These were therefore used to divide the electrode penetrations in these areas into representational sites and background sites. Additional method descriptions are in *Supporting Text*.

This work was supported by a Swedish Science Council grant (to P.E.R.) and by the K. A. Wallenberg Foundation.

1. Rockland, K. S. & Pandya, D. N. (1979) *Brain Res.* **179,** 3–20.
2. Engel, A. K., Fries, P. & Singer, W. (2001) *Nat. Rev. Neurosci.* **2,** 704–716.
3. Blakemore, C. & Tobin, E. A. (1972) *Exp. Brain Res.* **15,** 439–440.
4. Gilbert, C. D. & Wiesel, T. N. (1990) *Vision Res.* **30,** 1689–1701.
5. Hupé, J. M., James, A. C., Girard, P., Lomber, S. G., Payne, B. R. & Bullier, J. (2001) *J. Neurophysiol.* **85,** 134–145.
6. Roland, P. E. (2002) *Trends Neurosci.* **25,** 183–190.
7. Cohen, L. B., Salzberg, B. M., Davila, H. V., Ross, W. N. & Landowne, D. (1974) *J. Membr. Biol.* **19,** 1–36.
8. Grinvald, A., Lieke, E. E., Frostig, R. D. & Hildesheim, R. (1994) *J. Neurosci.* **14,** 2545–2568.
9. Seidemann, E., Arieli, A., Grinvald, A. & Slovin, H. (2002) *Science* **295,** 862–865.
10. Petersen, C. C. H., Grinvald, A. & Sakmann, B. (2003) *J. Neurosci.* **23,** 1298–1309.
11. Grinvald, A. & Hildesheim, R. (2004) *Nat. Rev. Neurosci.* **5,** 873–885.
12. Manger, P. R., Kiper, D., Masiello, I., Murillo, L., Tettoni, L., Hunyadi, Z. & Innocenti, G. M. (2002) *Cereb. Cortex* **12,** 423–437.
13. Kleinfeld, D. & Delaney, K. R. (1996) *J. Comp. Neurol.* **375,** 89–108.
14. de Curtis, M., Takashima, I. & Iijima, T. (1999) *Brain Res.* **837,** 314–319.
15. Weliky, M. (2000) *Neuron* **27,** 427–430.
16. Felleman, D. J. & Van Essen, D. C. (1991) *Cereb. Cortex* **1,** 1–47.
17. Guillery, R. W., Ombrellaro, M. & LaMantia, A. L. (1985) *Brain Res.* **352,** 221–233.
18. Claps, A. & Casagrande, V. A. (1990) *Brain Res.* **530,** 126–129.
19. Casanova, C. (2004) in *The Visual Neurosciences*, eds. Chalupa, L. M. & Werner, J. S. (MIT Press, Cambridge, MA), Vol. 1, pp. 592–609.
20. Arieli, A., Sterkin, A., Grinvald, A. & Aertsen, A. (1996) *Science* **273,** 1868–1871.
21. Ermentrout, G. B. & Kleinfeld, D. (2001) *Neuron* **29,** 33–44.
22. Petersen, C. C. H., Hahn, T. T. G., Mehta, M., Grinvald, A. & Sakmann, B. (2003) *Proc. Natl. Acad. Sci. USA* **100,** 13638–13643.
23. Prechtl, J. C., Bullock, T. H. & Kleinfeld, D. (2000) *Proc. Natl. Acad. Sci. USA* **97,** 877–882.
24. Senseman, D. M. & Robbins, K. A. (2002) *J. Neurphysiol.* **87,** 1499–1514.
25. Cauller, L. J. & Connors, B. W. (1994) *J. Neurosci.* **14,** 751–762.
26. Schroeder, C. E., Mehta, A. D. & Givre, S. J. (1998) *Cereb. Cortex* **8,** 575–592.
27. Cantone, G., Xiao, J., McFarlane, N. & Levitt, J. B. (2005) *J. Comp. Neurol.* **487,** 312–331.
28. von Stein, A., Chiang, C. & König, P. (2000) *Proc. Natl. Acad. Sci. USA* **97,** 14748–14753.
29. Baylis, G. C. & Driver, J. (2001) *Nat. Neurosci.* **4,** 937–942.
30. Lamme, V. A. F. (1995) *J. Neurosci.* **15,** 1605–1615.
31. Kandil, F. I. & Fahle, M. (2001) *Eur. J. Neurosci.* **13,** 2004–2008.
32. Innocenti G. M., Manger P. R., Masiello, I., Colin, I. & Tettoni, L. (2002) *Cereb. Cortex* **12,** 411–422.